DOI: 10.1002/ejic.201001149

One-Pot Synthesis of Carboxyl-Functionalized Rare Earth Fluoride Nanocrystals with Monodispersity, Ultrasmall Size and Very Bright Luminescence

Xuejin Wu,[a] Qingbin Zhang,[a] Xin Wang,*[a,b] Hui Yang,[a] and Yimin Zhu[a]

Keywords: Rare earths / Fluorides / Nanoparticles / Luminescence

We demonstrated a straightforward approach to the synthesis of ultrasmall, monodisperse and carboxyl-functionalized rare earth (RE) fluoride nanocrystals via a one-pot reaction by introducing poly(acrylic acid) (PAA) as a coordination agent and surfactant. The morphologies, crystal structure, surface groups, and luminescent properties of the PAA-capped RE fluoride nanocrystals were investigated in detail by TEM, FTIR, and photoluminescence spectroscopy. The obtained RE fluoride nanocrystals were ultrasmall in size, monodisperse, and highly crystalline. FTIR spectra confirmed that the PAA molecules strongly coordinated to the surface of the nanocrystals, which allows the formation of transparent colloidal aqueous solutions. Successful coating of the LaF_3 shell on the $NaCeF_4$:Tb^{3+} nanocrystals can increase the luminescence efficiency and lifetimes of Tb^{3+} ions relative to the pure $NaCeF_4$:Tb^{3+} core. This synthesis procedure could become a versatile approach for the straightforward synthesis of carboxyl-functionalized nanocrystals with ultrasmall size and monodispersity.

1. Introduction

Nanocrystals doped with Rare Earths (RE) have been extensively investigated for their potential applications in optics, optoelectronics, and biolabeling owing to their attractive features: photochemical stability, low toxicity, large Stokes shifts, long lifetime, and so forth.[1–5] Recently, RE fluoride nanocrystals with unique optical properties have become a new focus of research because of their high chemical stability and good solid solubility for optically active RE codopants.[2,6] To date, various synthesis approaches have been reported to successfully obtain the RE fluoride nanocrystals.[6–8] Most of these synthesis approaches involved the use of high-boiling organic solvents, such as oleic acid, 1-octadecene, and oleylamine. Although the colloidal nanoparticles synthesized using high-boiling organic solvents have high-quality crystallinity, narrow size distribution, and tunable shape, their hydrophobicity in nature and lack of surface functional groups (–COOH, $–NH_2$, or –SH) limit their application in significant fields, such as bioassay, imaging, and therapy.

To achieve their application in biomedical fields, the nanocrystals should be functionalized with water-soluble and biocompatible groups. To date, several strategies have been developed to modify the surface property from hydrophobicity to hydrophilicity for the nanocrystals synthesized in organic solvents, including ligand exchange,[9] ligand oxidation,[10–11] and encapsulation with SiO_2[12–13] (amphiphilic copolymer[14–15] or albumin[16]). Although many of these strategies can achieve water dispersibility, the procedures involved in the two-step post-functionalizing approaches are considerably complicated and time-consuming. However, a one-pot synthesis of water-soluble and biocompatible nanocrystals can provide a simple and straightforward strategy for surface functionalization. To avoid the sophisticated phase transition process, the development of a facile one-pot approach is required.

Herein, we demonstrate a straightforward synthesis of carboxyl-functionalized RE fluoride nanocrystals via one-pot reaction by means of a modified polyol process,[17] in which PAA was introduced in diethylene glycol (DEG). In the reaction process, PAA played the double role of surfactant and coordination agent to control nanocrystal growth and provide the nanocrystal water-solubility and biocompatibility. Some of the carboxyl groups on the PAA chains strongly coordinated to the surface of the fluoride nanocrystals, whereas the uncoordinated carboxyl groups contributed to the dispersibility of the nanocrystals in aqueous solution and surface functionalization for bioconjugation. The PAA-capped RE fluoride ($NaCeF_4$:Tb^{3+} and LaF_3:Ce^{3+}/Tb^{3+}) nanocrystals were characterized by transmission electron microscopy (TEM), X-ray diffraction (XRD), and Fourier transform infrared (FTIR) spectroscopy. The luminescence properties of the nanocrystals

[a] Suzhou Institute of Nano-Tech and Nano-Bionics, Chinese Academy of Sciences,
Suzhou 215123, China
Email: xwang2008@sinano.ac.cn
[b] Key Laboratory of Biogeology and Environmental Geology of Ministry of Education, CUG,
Wuhan 430074, P.R. China

Supporting information for this article is available on the WWW under http://dx.doi.org/10.1002/ejic.201001149.

dispersed in water were also investigated in detail. A $NaCeF_4$:Tb^{3+}/LaF_3 core/shell nanostructure was successfully synthesized to enhance the luminescence efficiency.

2. Results and Discussion

2.1 Morphologies and Structures of the RE Fluoride Nanocrystals

The morphologies, sizes, and structures of as-synthesized samples were examined by TEM. Figure 1 (a–f) displays typical TEM and high-resolution TEM images of $NaCeF_4$:Tb^{3+} (Figure 1, a–c) and $NaCeF_4$:Tb^{3+}/LaF_3 core/shell (Figure 1, d–f) nanocrystals. The high-resolution TEM images clearly show that the nanocrystals have uniform size, are monodisperse in water, and have an average diameter of 3.8 ± 0.8 nm and 6.8 ± 1.5 nm, respectively, corresponding to $NaCeF_4$:Tb^{3+} and $NaCeF_4$:Tb^{3+}/LaF_3 core/shell nanocrystals. The magnified TEM images further exhibit their approximately spherical shape (Figure 1, b and e). The high-resolution TEM image shown in Figure 1 (c) clearly exhibits the lattice fringes of the $NaCeF_4$ nanocrystals. The calculated interplanar distance is about 0.31 nm, corresponding to the d-spacing for the (101) lattice planes. Figure 1 (f) illustrates the apparent increase in size of the core/shell structure, suggesting the formation of the LaF_3 shell on the surface of the $NaCeF_4$ core.

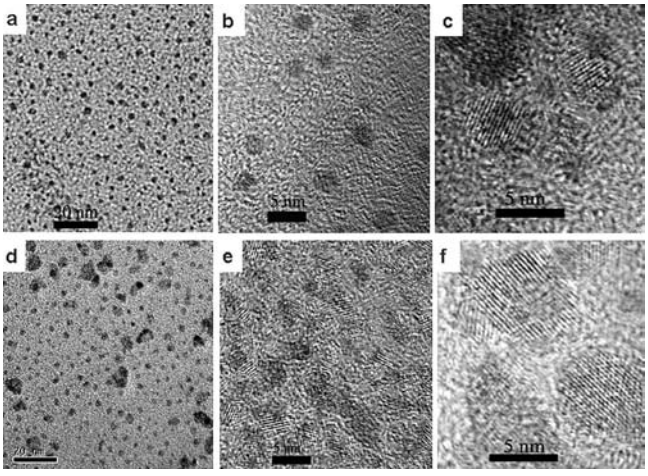

Figure 1. Typical TEM images; magnified TEM images; and high-resolution TEM images of $NaCeF_4$:Tb^{3+} (a–c) and $NaCeF_4$:Tb^{3+}/LaF_3 core/shell (d–f) nanocrystals.

The crystal structures of the samples were examined by powder XRD. Figure 2 shows the XRD patterns of the $NaCeF_4$:Tb^{3+} and $NaCeF_4$:Tb^{3+}/LaF_3 core/shell nanocrystals as well as the standard data of bulk $NaCeF_4$ and LaF_3. The positions and relative intensities of all diffraction peaks in Figure 2 (a) match well with the hexagonal phase structure known from the bulk $NaCeF_4$ crystals (JCPDS No. 50–0154). The XRD patterns indicate that the $NaCeF_4$ nanoparticles are highly crystalline in nature. Compared with Figure 2 (a), part b shows not only the diffraction peaks of the $NaCeF_4$ core but also those of the LaF_3 shell with a hexagonal crystalline structure (JCPDS No. 72-1435). Moreover, the XRD pattern in Figure 2 (b) corresponding to the LaF_3 shell is superior to that of $NaCeF_4$. No obvious shift of diffraction peaks was observed due to the broadening of the XRD peak of the nanosized crystals. It should be pointed out that small amounts of NaF component emerged in the pattern of Figure 2 (b) due to the excessive amounts of NH_4F and NaOH used in the reaction system.[8]

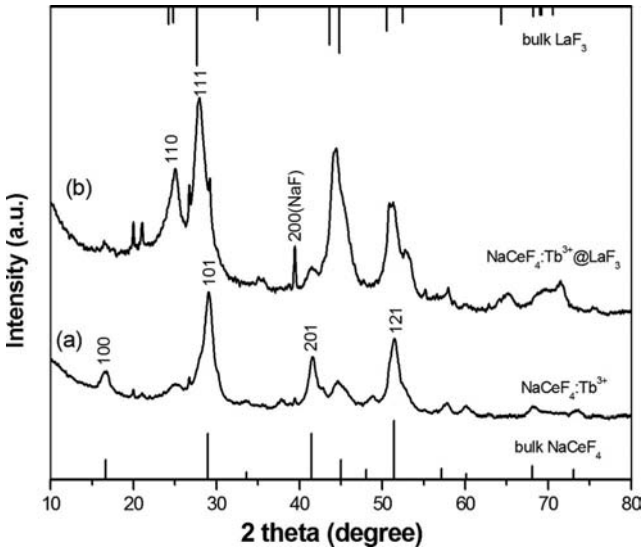

Figure 2. Powder XRD patterns of (a) $NaCeF_4$:Tb^{3+}, and (b) $NaCeF_4$:Tb^{3+}/LaF_3 core/shell nanocrystals. The line spectra correspond to the standard data of bulk $NaCeF_4$ (JCPDS No. 50–0154) and LaF_3 (JCPDS No. 72–1435), respectively.

2.2 FTIR Spectra

FTIR spectroscopy was performed to characterize the organic functional groups located on the nanocrystal surface. Figure 3 shows the FTIR spectra of the pure PAA powder and the as-prepared products, respectively. As shown in part a of Figure 3, a strong absorption band at 1720 cm^{-1} is assigned to the C=O stretching mode of free carboxylic acid groups (–COOH), while weaker bands centered at 1455 and 1415 cm^{-1} are associated with the scissor and bending vibrations of $–CH_2–$ and CH–CO groups,[18] respectively. FTIR spectra of the PAA-capped $NaCeF_4$:Tb^{3+} and $NaCeF_4$:Tb^{3+}/LaF_3 nanocrystals are shown in Figure 3 (b and c, respectively). In comparison with pure PAA, a strong band due to the C=O stretching mode from carboxyl groups was shifted from 1720 to 1730 cm^{-1} after the carboxyl groups of PAA strongly coordinated to RE ions. However, both parts b and c of Figure 3 show a new band centered at 1573 cm^{-1}, which provides direct evidence of the attachment of PAA molecules to the nanocrystal surface. The two bands at 1573 cm^{-1} and 1455 cm^{-1} are assigned to the asymmetric and symmetric stretching vibration modes of the carboxyl group of PAA, respectively, suggesting the PAA capping on the nanocrystal surface through the $–COO–RE^{3+}$ bonds. Because the for-

mation of a coordination bond of carboxyl with RE ions diminished the charge density on the carboxyl oxygen, the vibration band of asymmetric vibration absorption of the carboxyl group shifted to the lower wavenumber of 1575–1415 cm^{-1}. As is noted, the 1455 cm^{-1} band may be the result of overlap between the $\nu(COO^-)$ vibrational stretching and $\delta(CH_2)$ scissoring bands. It is clear that a large amount of the carboxyl groups in the PAA chains strongly coordinated to the nanocrystal surface.

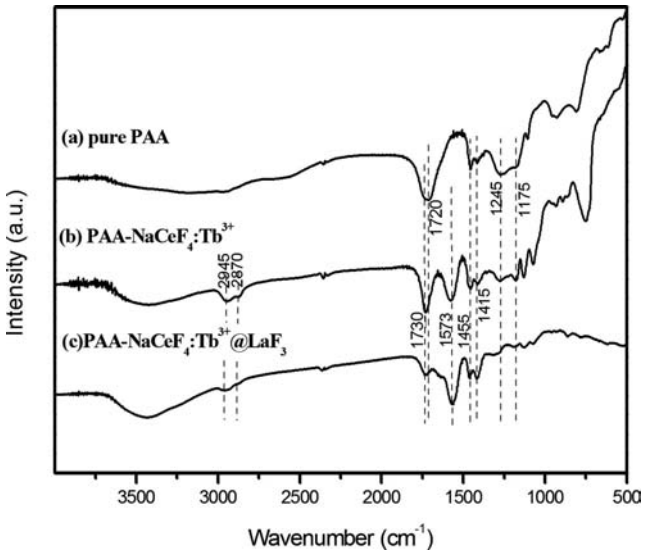

Figure 3. FTIR spectra of: (a) pure PAA powder, (b) PAA-capped $NaCeF_4:Tb^{3+}$, (c) PAA-capped $NaCeF_4:Tb^{3+}/LaF_3$ core/shell nanocrystals.

2.3 Synthesis of PAA-Capped RE Fluoride Nanocrystals

In this work, a modified polyol approach was developed to produce the carboxyl-functionalized RE fluoride luminescence nanocrystals by introducing PAA in DEG via a one-pot reaction. The hydrophilic PAA played two crucial roles: not only as a coordination agent, which rendered the carboxyl-functionalized nanocrystals, but also as a surfactant, which controlled the shape and size of the nanocrystals. The formation of RE fluorides, taking $NaCeF_4:Tb^{3+}$ as an example, is illustrated in Scheme 1. When PAA was added to the reaction system, an intermediate PAA-RE^{3+} complex was formed through the chelating interaction between carboxylic groups and RE^{3+} ions. During the heating process, the chelating of the PAA-RE^{3+} complex was weakened and RE^{3+} ions were released gradually from the complexes. Once a sufficient amount of fluoride ions had been injected rapidly into the reaction system, small nuclei of $NaCeF_4$ were produced by the coprecipitation reaction between Na^+, RE^{3+}, and F^- ions. Under high-temperature conditions the well-known Ostwald ripening process dominated the growth of the nanocrystals. During the growth process, however, higher concentrations of PAA effectively inhibited the growth of $NaCeF_4$ nanocrystals, resulting in a relatively smaller size, narrower size distribution, and more regular spherical shape than those synthesized at lower concentrations (Figure S1). After the reaction had completed, the nanocrystal surface was capped by PAA via a strong chelating interaction between carboxyl acid groups and RE^{3+} ions. The possible formation mechanism of the $NaCeF_4$ nanocrystals has been summarized and is available in the Supporting Information.

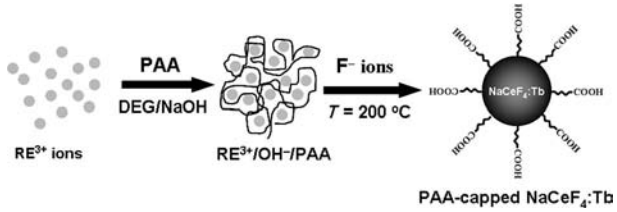

Scheme 1. Schematic synthesis of PAA-capped $NaCeF_4:Tb^{3+}$ nanocrystals.

To examine whether this approach is versatile, fluoride $LaF_3:Ce^{3+}/Tb^{3+}$ nanocrystals were also obtained by a similar preparation procedure (see Supporting Information). The hexagonal-phase LaF_3 nanocrystals were identified from the XRD patterns (Figure S2) and their average size is around 4.0 ± 0.8 nm observed in the TEM images (Figure S3). It should be noted that the amount of NaOH used in preparing $NaCeF_4$ was twice that for the preparation of LaF_3. In addition, Li et al. reported that the molar mass of NaOH for the synthesis of $NaCeF_4$ was twice that of KOH for the synthesis of CeF_3 nanocrystals in a similar reaction system.[19] These similar results indicate that the amount of hydroxy ions may be an important parameter for nucleation and growth of the $NaCeF_4$ nanocrystals. However, determination of the intrinsic role that the NaOH reagent plays in the formation of $NaCeF_4$ is still challenging and needs to be further investigated.

The formation of the $NaCeF_4:Tb^{3+}/LaF_3$ core/shell structure is illustrated in Figure S4, and it can be divided into two steps. First, the as-prepared $NaCeF_4:Tb^{3+}$ and PAA were dispersed in the NaOH/DEG stock solution. When the La^{3+} and F^- ions were added to the above solution, the PAA-La^{3+} complex was formed rapidly. However, under high-temperature conditions, the chelating of the PAA-La^{3+} complex was weakened. The released La^{3+} ions then reacted with the F^- ions in the solution to produce LaF_3 nuclei on the surface of $NaCeF_4:Tb^{3+}$ which acted as a seed for LaF_3 growth. In the second step, the LaF_3 nuclei on the $NaCeF_4:Tb^{3+}$ surface aggregated to form the LaF_3 shell, which resulted in a $NaCeF_4:Tb^{3+}/LaF_3$ core/shell structure.

2.4 Photoluminescence Properties

The as-synthesized $NaCeF_4:Tb^{3+}$and $NaCeF_4:Tb^{3+}/LaF_3$ nanocrystals can be dispersed in water to form transparent colloidal solutions (Figure S5). Bright green emissions from these colloidal solutions could be seen under 254-nm UV lamp irradiation, as shown in Figure S5. The Ce^{3+} ions can absorb irradiative light and transfer the en-

ergy to Tb^{3+} ions because an energy transfer between Ce^{3+} and Tb^{3+} ions occurs easily. Thus, a strong green emission from Tb^{3+} ions can be detected. Figure 4 depicts the excitation and emission spectra of the $NaCeF_4$:Tb^{3+} nanocrystals in aqueous solution. The excitation spectrum (λ_{em} = 544 nm) in Figure 4 (a) shows an excitation peak at around 248 nm, attributed to the absorption of 4f-5d electronic transitions of Ce^{3+} ions. As shown in Figure 4 (b), the four main peaks of the emission spectrum in the range 450–650 nm are assigned to the $^5D_4 \rightarrow {}^7F_J$ (J = 6–3) transitions of Tb^{3+} ions under 248 nm excitation.[7,20] In addition, similar luminescent properties were also observed in the LaF_3:Ce^{3+}/Tb^{3+} solution (Figure S6). The quantum yield (QY) is an important parameter to characterize the luminescent efficiency of RE fluoride nanocrystals. A QY of 24% was evaluated for the Tb^{3+} emission of $NaCeF_4$:Tb^{3+} nanocrystals based on a relative method with reference to that of Rhodamine 6G (see Supporting Information).[21] It should be pointed out that our result is lower than that of the reported results [$CePO_4$:Tb^{3+} (43%)[20] and GdOF:Ce^{3+}/Tb^{3+}(40%)[22]] in organic solvent because high-energy vibrations of water molecules efficiently quench the excited state of the Tb^{3+} ions.

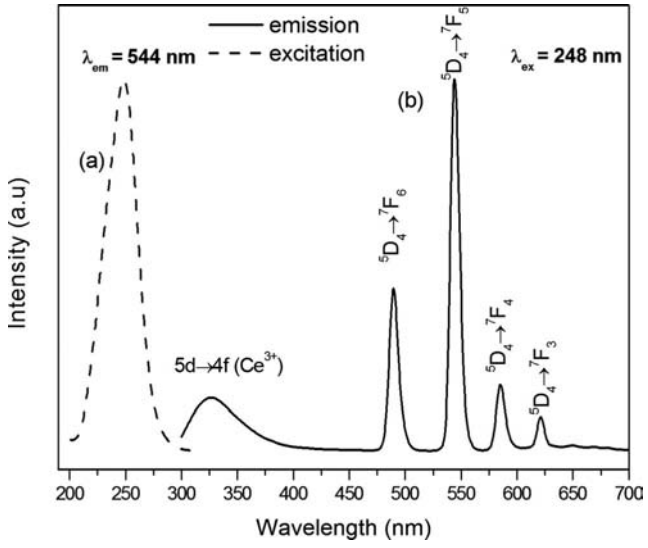

Figure 4. The excitation (a) and emission (b) spectra of the colloidal solution of $NaCeF_4$:Tb^{3+} nanocrystals.

For the nanocrystals with diameters less than 10 nm, it is a fact that a large fraction of dopant ions are located on surface sites and are prone to quenching by absorbed species such as –COOH or –OH with high-energy vibrations. Consequently, a general strategy has been accepted to design the core/shell structure to enhance the luminescent efficiency by protecting the luminescent ions from other quenching sites existing on the surface. As shown in Figure 5, identical profiles were observed from the characteristic emission of the $^5D_4 \rightarrow {}^7F_J$ (J = 6–3) transitions of Tb^{3+} ions for the $NaCeF_4$:Tb^{3+} and $NaCeF_4$:Tb^{3+}/LaF_3 core/shell nanocrystals, however, the emission intensity of the core/shell structure was evidently enhanced with respect to that of the core. At the same time, after successfully coating with the thin shell of LaF_3, the QY of the core/shell structure increased to 62%, which is close to the reported value in $CePO_4$:Tb^{3+}/$LaPO_4$ nanostructures.[20] The increase of QY should be attributed to the coating of the LaF_3 shell which could effectively reduce nonradiative quenching of the luminescent RE ions by surface defects and surrounding solvent molecules. In addition, the shielding effect of the LaF_3 shell also protects against the oxidation of Ce^{3+} in $NaCeF_4$:Tb^{3+} nanocrystals to Ce^{4+}. Although $NaCeF_4$:Tb^{3+} dispersed in deionized water formed a transparent colloidal solution, a shallow yellow solution was observed after storing the as-synthesized sample for only a few months (Figure S5a). In contrast, the colloidal aqueous solution containing the core/shell structure nanocrystals remained colorless (Figure S5c) and no variation was observed in their luminescent emission intensity over longer time periods (Figure S5d), providing additional evidence of the formation of the core/shell structure.

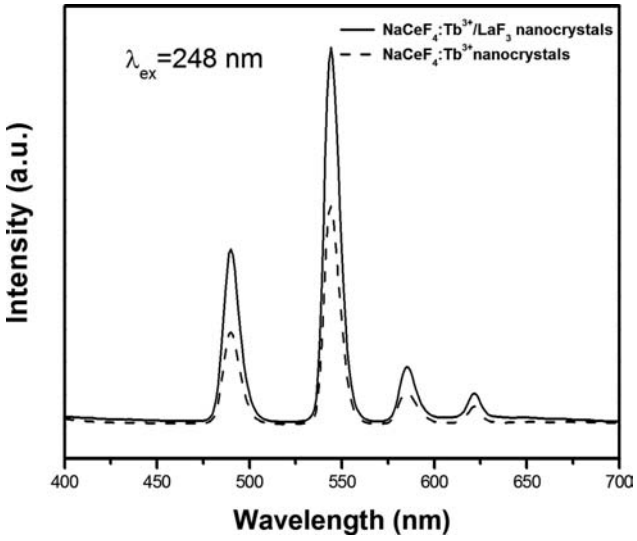

Figure 5. The emission spectra of the colloidal solution of $NaCeF_4$:Tb^{3+} (dashed line) and $NaCeF_4$:Tb^{3+}/LaF_3 core/shell (solid line) nanocrystals, respectively.

To further confirm the enhancement of luminescent efficiency, the lifetimes were also investigated by comparing the decay of luminescence of the two samples. Figure 6 shows the luminescence decay curves of 544 nm emission from $^5D_4 \rightarrow {}^7F_5$ of Tb^{3+} in $NaCeF_4$ and $NaCeF_4$/LaF_3 nanocrystals in aqueous solutions, respectively. The two curves can be well fitted using a double-exponential function based on the formula: $I = I_1 \exp(-t/\tau_1) + I_2 \exp(-t/\tau_2)$ (τ_1 and τ_2 correspond to the long and short component of lifetimes of Tb^{3+} ions).[23] The lifetimes of τ_1 = 4.6 ms (79%), τ_2 = 1.3 ms (21%) and τ_1 = 5.9 ms (84%), τ_2 = 1.8 ms (16%) were estimated for the $NaCeF_4$:Tb^{3+} core and the $NaCeF_4$:Tb^{3+}/LaF_3 core/shell structure, respectively. The dramatic increase of the lifetime demonstrated that the nonradiative process has been greatly diminished by the shield effect of the LaF_3 shell. Furthermore, it is noteworthy that an increase of lifetime was self-consistent with an enhance-

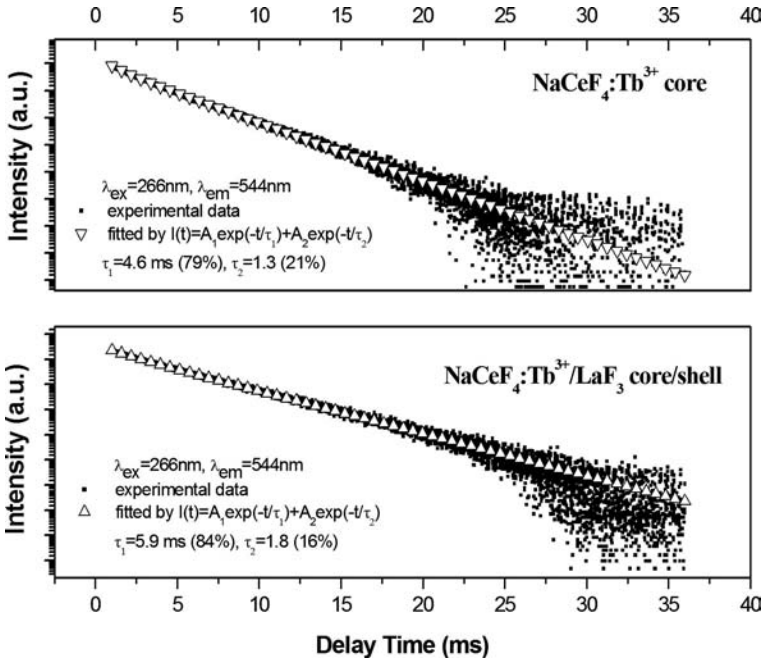

Figure 6. Luminescence decay curves (λ_{em} = 544 nm) from Tb^{3+} ions in $NaCeF_3$:Tb^{3+} and $NaCeF_3$:Tb^{3+}/LaF_3 core/shell samples (λ_{ex} = 266 nm), respectively.

ment of luminescent QY after the growth of a thin shell around the core. Both results provide evidence of the formation of the $NaCeF_4$:Tb^{3+}/LaF_3 core/shell structure.

3. Conclusion

In conclusion, ultrasmall, monodisperse, carboxyl-functionalized RE fluoride nanocrystals were synthesized by introducing PAA as both coordination agent and surfactant. PAA served important roles in not only precisely controlling the growth of the nanocrystals but also directly functionalizing the nanocrystals based on the coordination of carboxyl acid groups with RE atoms on the surface. Therefore, the PAA-capped RE fluoride nanocrystals can be well-dispersed in water to form transparent colloidal solutions. Furthermore, after coating with a shield shell of LaF_3, the luminescent efficiency and lifetimes of the $NaCeF_4$:Tb^{3+}/LaF_3 nanocrystals were greatly improved in comparison to the bare $NaCeF_4$:Tb^{3+} nanocrystals due to suppression of the nonradiative processes and reduction of other kinds of surface quenchers. It is expected that this simple, flexible, and effective approach could be extended to synthesizing various kinds of carboxyl-functionalized nanocrystals for bioassay and bioimaging applications.

4. Experimental Section

Materials: Poly(acrylic acid) (PAA, *Mw* = 1800) was obtained from Sigma–Aldrich. Sodium hydroxide (NaOH, 98.8%) was purchased from Alfa Aesar. $Ce(NO_3)_3$ (99.99%), ammonium fluoride (NH_4F, 99.99%), diethylene glycol (DEG, 99%, AR), and ethyl alcohol were purchased from Sinopharm Chemical Reagent Co. $La(NO_3)_3$ and $Tb(NO_3)_3$ were purchased from Beijing Lanthanide Creative Co. Ltd. All chemicals were directly used as received without further treatment.

Synthesis of PAA-Capped $NaCeF_4$:Tb^{3+} Nanocrystals: The PAA-capped $NaCeF_4$:Tb^{3+} nanocrystals were synthesized by using a modified polyol process.[17] A mixture of DEG (20 mL) and NaOH (10 mmol) was heated at 200 °C for 30 min in an argon atmosphere and then cooled to room temperature. Sequentially, $Ce(NO_3)_3$ (0.85 mmol), $Tb(NO_3)_3$ (0.15 mmol), and PAA (1.0 mmol) were added and heated at 200 °C for 10 min, thus forming a transparent light-yellow solution. At this temperature, a solution of DEG (5 mL) containing NH_4F (4.5 mmol) was injected, maintained at 200 °C for an hour, and then cooled to room temperature naturally. After adding ethanol, the as-synthesized products were precipitated by centrifuging at 12000 rpm for 20 min and then washed several times with water and ethanol. The final solid precipitation could be easily dispersed in water to form a transparent colloidal aqueous solution.

Synthesis of PAA-Capped $NaCeF_4$:Tb^{3+}/LaF_3 Core/Shell Nanostructure: Typically, a solution of DEG (20 mL) containing PAA (0.5 mmol), NaOH (5.0 mmol), La $(NO_3)_3$ (0.5 mmol), and the as-prepared $NaCeF_4$:Tb^{3+} was heated at 200 °C for 10 min. At this temperature, a solution of DEG (2.0 mL) mixed with NH_4F (2.3 mmol) was injected into the reaction system, and the reaction temperature was then maintained at 200 °C for an hour. The procedures that followed were the same as that for $NaCeF_4$:Tb^{3+}. The PAA-capped $NaCeF_4$:Tb^{3+}/LaF_3 core/shell nanostructures were obtained and, finally, can be well dispersed in water.

Characterizations: TEM and high-resolution TEM were performed with a FEI Tecnai G2 F20 S-Twin at 200 kV and images were acquired digitally with a Gatan multiple CCD camera. Power XRD measurements were performed with a X′Pert-Pro MPD diffractometer equipped with graphite-monochromated Cu-K_α radiation (λ = 0.15406 nm). FTIR spectra were measured with a Thermo Nicolet 6700 FTIR spectrometer. The UV/Vis absorption spectra were measured with a Perkin–Elmer (Lambda 25) spectrophotome-

ter using a quartz cell with a width of 1 cm. The excitation and emission spectra were recorded with a Hitachi F-4600 spectrophotometer. The time-resolved fluorescence investigations were performed following excitation with a 266 nm light generated from a fourth-harmonic generator pumped by a pulsed Nd:YAG laser with a line width of 1.0 cm^{-1}, a pulse duration of 10 ns, and a repetition frequency of 10 Hz. The signals corresponding to decay curves of the Tb^{3+} ion emission (544 nm) obtained by a photomultiplier (Hamamatsu R928) attached to the spectrometer (Jobin–Yvon TRIAX550) were collected by a Tektronix TDS 3052 500-MHz digital real-time storage oscilloscope.

Supporting Information (see footnote on the first page of this article): SEM images of $NaCeF_4$:Tb^{3+} at the low amount of PAA; synthesis procedure of LaF_3:Ce^{3+}/Tb^{3+} nanocrystals; XRD pattern, TEM images, and luminescence properties of LaF_3:Ce^{3+}/Tb^{3+} nanocrystals; photographs and luminescence images of $NaCeF_4$:Tb^{3+} and NaCeF4:Tb^{3+}/LaF_3; formation mechanism of PAA-capped $NaCeF_4$:Tb^{3+}; scheme of formation of $NaCeF_4$:Tb^{3+}/LaF_3 core/shell nanocrystals; and details for the quantum yield calculation.

Acknowledgments

The work was financially supported by the National Natural Science Foundation of China (NSFC) (grant number 10804082), the Fund of Excellent President Award of the Chinese Academy of Sciences (2008), and the open fund of the Key Laboratory of Biogeology and Environmental Geology of the Ministry of Education (BGEG1004). The authors greatly thank Prof. Xianggui Kong, Prof. Guiye Shan and Dr. Xiaomin Liu for the XRD data and lifetime measurements.

[1] P. R. Diamente, M. Raudsepp, F. van Veggel, *Adv. Funct. Mater.* **2007**, *17*, 363–368.
[2] F. Wang, Y. Han, C. S. Lim, Y. H. Lu, J. Wang, J. Xu, H. Y. Chen, C. Zhang, M. H. Hong, X. G. Liu, *Nature* **2010**, *463*, 1061–1065.
[3] H. S. Qian, H. C. Guo, P. C. L. Ho, R. Mahendran, Y. Zhang, *Small* **2009**, *5*, 2285–2290.
[4] X. Wang, X. G. Kong, G. Y. Shan, Y. Yu, Y. J. Sun, L. Y. Feng, K. F. Chao, S. Z. Lu, Y. J. Li, *J. Phys. Chem. B* **2004**, *108*, 18408–18413.
[5] L. Y. Wang, R. X. Yan, Z. Y. Hao, L. Wang, J. H. Zeng, H. Bao, X. Wang, Q. Peng, Y. D. Li, *Angew. Chem. Int. Ed.* **2005**, *44*, 6054–6057.
[6] H. X. Mai, Y. W. Zhang, R. Si, Z. G. Yan, L. D. Sun, L. P. You, C. H. Yan, *J. Am. Chem. Soc.* **2006**, *128*, 6426–6436.
[7] J. C. Boyer, J. Gagnon, L. A. Cuccia, J. A. Capobianco, *Chem. Mater.* **2007**, *19*, 3358–3360.
[8] L. Y. Wang, Y. D. Li, *Chem. Mater.* **2007**, *19*, 727–734.
[9] J. C. Boyer, M. P. Manseau, J. I. Murray, F. van Veggel, *Langmuir* **2010**, *26*, 1157–1164.
[10] Z. G. Chen, H. L. Chen, H. Hu, M. X. Yu, F. Y. Li, Q. Zhang, Z. G. Zhou, T. Yi, C. H. Huang, *J. Am. Chem. Soc.* **2008**, *130*, 3023–3029.
[11] H. P. Zhou, C. H. Xu, W. Sun, C. H. Yan, *Adv. Funct. Mater.* **2009**, *19*, 3892–3900.
[12] S. Sivakumar, P. R. Diamente, F. C. van Veggel, *Chem. Eur. J.* **2006**, *12*, 5878–5884.
[13] Q. Lu, F. Y. Guo, L. Sun, A. H. Li, L. C. Zhao, *J. Appl. Phys.* **2008**, *103*, 123533–123543.
[14] R. Naccache, F. Vetrone, V. Mahalingam, L. A. Cuccia, J. A. Capobianco, *Chem. Mater.* **2009**, *21*, 717–723.
[15] E. N. M. Cheung, R. D. A. Alvares, W. Oakden, R. Chaudhary, M. L. Hill, J. Pichaandi, G. C. H. Mo, C. Yip, P. M. Macdonald, G. J. Stanisz, F. van Veggel, R. S. Prosser, *Chem. Mater.* **2010**, *22*, 4728–4739.
[16] D. J. Naczynski, T. Andelman, D. Pal, S. Chen, R. E. Riman, C. M. Roth, P. V. Moghe, *Small* **2010**, *6*, 1631–1640.
[17] C. Feldmann, *Adv. Funct. Mater.* **2003**, *13*, 101–107.
[18] M. A. Moharram, M. G. Khafagi, *J. Appl. Polym. Sci.* **2007**, *105*, 1888–1893.
[19] S. A. Li, T. Xie, Q. Peng, Y. D. Li, *Chem. Eur. J.* **2009**, *15*, 2512–2517.
[20] K. Kompe, H. Borchert, J. Storz, A. Lobo, S. Adam, T. Moller, M. Haase, *Angew. Chem. Int. Ed.* **2003**, *42*, 5513–5516.
[21] K. Hanaoka, K. Kikuchi, H. Kojima, Y. Urano, T. Nagano, *J. Am. Chem. Soc.* **2004**, *126*, 12470–12476.
[22] Y. P. Du, Y. W. Zhang, L. D. Sun, C. H. Yan, *J. Phys. Chem. C* **2008**, *112*, 405–415.
[23] J. W. Stouwdam, M. Raudsepp, F. van Veggel, *Langmuir* **2005**, *21*, 7003–7008.

Received: October 27, 2010
Published Online: March 16, 2011

